Catalysis Today 165 (2011) 71–79

Contents lists available at ScienceDirect

Catalysis Today

journal homepage: www.elsevier.com/locate/cattod

An understanding of chemoselective hydrogenation on crotonaldehyde over Pt(1 1 1) in the free energy landscape: The microkinetics study based on first-principles calculations

Xiao-Ming Cao, Robbie Burch, Chris Hardacre, P. Hu*

School of Chemistry and Chemical Engineering, The Queen's University of Belfast, Belfast BT9 5AG, UK

ARTICLE INFO

Article history:
Received 30 September 2010
Received in revised form
13 December 2010
Accepted 15 December 2010
Available online 9 February 2011

Keywords:
DFT
Microkinetics
α,β-Unsaturated aldehydes
Crotonaldehyde
Pt(1 1 1)
Selective hydrogenation
Free energy landscape

ABSTRACT

Microkinetic model is developed in the free energy landscape based on density functional theory (DFT) to quantitatively investigate the reaction mechanism of chemoselective partial hydrogenation of crotonaldehyde to crotyl alcohol over Pt(1 1 1) at the temperature of 353 K. Three different methods (mobile, immobile and collision theory models) were carried out to obtain free energy barrier of adsorption/desorption processes. The results from mobile and collision theory models are similar. The calculated TOFs from both models are close to the experiment value. However, for the immobile model, in which the free energy barrier of desorption approaches the energy barrier, the calculated TOF is 2 orders of magnitude lower than the other models. The difficulty of adsorption/desorption may be overestimated in the immobile model. In addition, detailed analyses show that for the surface hydrogenation elementary steps, the entropy and internal energy effects are small under the reaction condition, while the zero-point-energy (ZPE) correction is significant, especially for the multi-step hydrogenation reaction. The total energy with the ZPE correction approaches to the full free energy calculation for the surface reaction under the reaction condition.

1. Introduction

Hydrogenation in heterogeneous catalysis has a great number of applications in bulk and fine chemical synthesis in both research laboratory and industrial scales. For example, they are essential steps for many commercially important reaction processes such as Fischer–Tropsch (FT) reactions [1–10] and ammonia synthesis [11–16]. Despite a wide range of applications and extensive studies, the selective hydrogenation of various reactants with multiple functional groups to desired products is still a challenging issue. The selective hydrogenation of α,β-unsaturated aldehydes (UAL) is one of such examples. Hydrogenation of UAL to the corresponding α,β-unsaturated alcohol (UOL) intermediates is a key step in fine chemical industry, mainly in the flavor and fragrance [17,18] and pharmaceutical industries [19]. Despite the significant research efforts [20–22] on simplified model molecules such as cinnamaldehyde, prenal, crotonaldehyde and acrolein which have been devoted to this subject in recent years, it is still a challenge to achieve high selectivity to UOL, particularly for some small molecules such as acrolein and crotonaldehyde. The reason is believed to be that saturated aldehydes (SAL) instead of desired UOL are thermodynamically favored hydrogenation products.

A significant experimental effort has been dedicated to locating catalysts over which hydrogenation on carbonyl bond instead of ethylenic bond is likely to be a preferential process. A variety of metals, e.g. Ru, Rh, Ni, Pd, Au and Pt, have been reported for chemoselective hydrogenation reaction [23–37]. Among them, platinum system is most extensively studied [38–42], which facilitates the comprehensive understanding of reaction mechanism over different metal catalysts.

In the early work, it prevailed that the ethylenic bond is kinetically easier to be hydrogenated than carbonyl bond [20] based on the lower bonding energy of ethylenic bond than that of carbonyl bond. Experimental work from the hydrogenation of acrolein over Pt supported this argument, in which unsaturated alcohol was rarely formed and the main product was propanal [43]. This was also in agreement with the results from theoretical studies on the competitive adsorption configuration of UAL [44,45] where the adsorption via carbonyl bond was not the favored chemisorption mode compared with that via ethylenic bond. However, recent DFT calculations on the partial hydrogenation of acrolein on Pt(1 1 1) from Loffreda et al. [46–48] showed that during the surface hydrogenation process, hydrogenation of carbonyl bond is kinetically favored following the so-called half Eley–Rideal mechanism. For acrolein, it was proposed that the desorption step in the carbonyl

* Corresponding author. Tel.: +44 (0)28 9097 4259; fax: +44 (0)28 9097 4687.
E-mail address: p.hu@qub.ac.uk (P. Hu).

0920-5861/$ – see front matter © 2011 Elsevier B.V. All rights reserved.
doi:10.1016/j.cattod.2010.12.056

hydrogenation pathway with a barrier of 104 kJ mol^{-1} (1.08 eV) is the rate-determining step [46]. Loffreda et al. suggested that this high barrier is responsible for the low ratio of unsaturated alcohol even though it is a preferential surface hydrogenation product.

However, it should be noted that the rate of adsorption/desorption step is strongly affected by the entropic factor [49,50]. The energy barriers directly from DFT calculations only provide the total energy landscape under the zero-temperature conditions, not including the entropic effect. Hence the variation of the entropy during the desorption procedure might be overlooked if the data from the energy landscape (0 K) are only used in the study of desorption process. It is essential to extend the study to the free energy landscape to investigate the significance of the desorption step on the chemoselective hydrogenation on crotonaldehyde.

It is worth mentioning that the detailed balance (or microscopic reversibility) is often neglected regarding describing adsorption/desorption processes. The adsorption and desorption processes are usually independently described. Collision theory is generally utilised to calculate the rate constant of the adsorption process, while the rate constant of the desorption process, is often described using the Arrhenius equation, in which the pre-exponential factor is directly assumed to be 10^{13} or an experimental value and the energy barrier comes from the DFT data in the total energy landscape [51–53]. The inconsistent treatment of the study of the forward and reverse processes is likely to lead to a result where the detailed balance breaks down. This is a trivial problem in some cases because adsorption/desorption step is sometimes not the rate-determining step in the reaction network [54]. However, in the present reaction system, the desorption rate of the product is regarded as a kinetically critical step. When the adsorption and desorption processes are both described in the free energy landscape, one is able to avoid the breakdown of detailed balance. In addition, although the total energy (0 K) directly from DFT is widely acknowledged to describe the surface procedure, especially for gas–solid reactions, the detailed error between total energy (0 K) and free energy landscape has never been quantitatively analyzed. It is also valuable to probe this issue.

Recently, microkinetic modeling based on DFT data has become a promising tool for systems with complex reaction networks. It provides the semiquantitative or quantitative kinetic understanding of the reaction mechanism with great clarity and simplicity. Hence this paper is dedicated to combining Gibbs free energy from DFT and statistical thermodynamic treatment with microkinetic modeling to understand the chemoselective hydrogenation of crotonaldehyde over Pt(1 1 1) at 353 K.

2. Theoretical methods

2.1. Density functional theory (DFT)

All periodic DFT calculations were carried out with the Perdew–Burke–Ernzerhof (PBE) generalized gradient approximation (GGA) functional [55] using Vienna ab initio simulation program (VASP) [56,57]. The projector-augmented-wave (PAW) pseudopotentials [58] were utilized to describe the core electron interactions and the plane-wave basis expansion cut-off was set to 400 eV. Metal surfaces were modeled by a periodic 4-layer slab with a ~12 Å vacuum region placed between periodically repeated slabs. A $p(3 \times 3)$ supercell was used with $3 \times 3 \times 1$ Monkhorst–Pack k-point mesh sampling for Brillouin zone integration. Previous calculations [46,47] have shown that the setup above is sufficient to obtain converged energy.

Geometry optimization was implemented by the quasi-Newton algorithm until all the remaining forces on each relaxed atoms were less than 0.01 eV/Å and the total energy convergency criteria for electronic SCF loop was set to 10^{-7} eV to accomplish the accurate vibrational frequencies. During all the optimization processes, the bottom two layers metal atoms were fixed in the slab while the top two layers and adsorbates were relaxed. Transition states (TSs) of all the reactions were located with DIMER method [59–61]. All the geometry structures have been confirmed by subsequent vibrational calculations yielding no imaginary frequencies for adsorption intermediates and only one imaginary frequency for transition states, respectively. The numerical calculation of the second derivatives of the harmonic potential energy surface provided the vibrational frequencies and corresponding normal modes. A geometrical displacement of 0.01 Å was utilized for all vibrational calculations.

2.2. Statistical treatment and reaction rate

The statistical mechanics based on Boltzmann distribution is followed by the explicit calculation of zero-point-energy (ZPE) entropy, internal energy and enthalpy derived from partition functions. Herein all the elementary rate constants are derived from transition state theory (TST). Despite the breakdown of rapid energy randomization [62] and the recrossings of trajectories [49], which is opposite to the underlying assumptions of TST [63], Pitt et al. [49] have demonstrated that TST is still capable of the depiction of adsorption/desorption process.

The rate constant k is defined in terms of TST as follows:

$$k = \frac{k_B T}{h} e^{-\Delta G^{\neq,\circ}/k_B T} = \frac{k_B T}{h} e^{\Delta S^{\neq,\circ}/k_B} e^{-\Delta H^{\neq,\circ}/k_B T}$$

$$= \frac{k_B T}{h} \frac{q^{\neq}}{q} e^{-(E_a + \Delta \mathrm{ZPE}^{\neq})/k_B T} = A e^{-E_a'/k_B T} \quad (1)$$

where k_B is Boltzmann constant, h is Planck's constant, E_a is the activation energy barrier from DFT. E_a' corresponds to the activation energy barrier with the ZPE correction. q and $q^{\neq}$ are the partition functions of initial state (IS) and TS, respectively. $\Delta G^{\neq,\circ}$, $\Delta H^{\neq,\circ}$, $\Delta S^{\neq,\circ}$ and $\Delta \mathrm{ZPE}^{\neq}$ are the changes of standard molar Gibbs free energy, enthalpy, entropy and zero-point-energy correction between TS and IS, respectively. A is pre-exponential factor.

For surface reactions, only vibration modes were taken into account. All the vibrational frequencies ν_i (Hz) were calculated based on the harmonic oscillators approximation [64]. The ZPE correction is calculated as follows [64]:

$$\mathrm{ZPE} = \sum_i \frac{h\nu_i}{2} \quad (2)$$

where h is Planck constant. The standard molar vibrational internal energy contribution is given by [64]

$$U^{\circ}_{\mathrm{vib}} = RT \sum_i \frac{h\nu_i/k_B}{e^{h\nu_i/k_B T} - 1} \quad (3)$$

where k_B is Boltzmann constant, R is gas constant. The standard molar vibrational entropy is calculated in terms of the following expression:

$$S^{\circ}_{\mathrm{vib}} = R \sum_i \left[\frac{h\nu_i/k_B T}{e^{h\nu_i/k_B T} - 1} - \ln(1 - e^{-h\nu_i/k_B T}) \right] \quad (4)$$

For the adsorption/desorption steps, the translational, rotational contributions are taken into account for gaseous species and TSs as well. For a gas molecule moving in the three-dimensional (3D) space, the standard molar translational internal energy is

$$U^{\circ}_{\mathrm{trans\text{-}3D}} = \frac{3}{2} RT \quad (5)$$

Table 1
Rate equations for the kinetic model based on reaction step i. As Scheme 1 displayed, CAL, COL, MS1, MS2 denote crotonaldehyde, crotyl alcohol, 1-hydroxycrotyl and crotyloxy, respectively. The species name followed by * denotes the species adsorbed on the surface. r_i, k_i and K_i denote the net rate, the forward rate constant and reaction equilibrium constant of elementary step i, respectively. P_x is the partial pressure of gaseous molecule x. θ_x is the coverage of species x and θ_* is the coverage of free sites.

Step i	Reaction elementary step	Rate equations
1	$CAL + * \rightleftharpoons CAL^*$	$r_1 = k_1 \frac{p_{cal}}{p^\circ}\theta_* - \frac{k_1}{K_1}\theta_{cal^*}$
2	$H_2 + 2^* \rightleftharpoons 2H^*$	$r_2 = k_2 \frac{p_{H_2}}{p^\circ}\theta_*^2 - \frac{k_2}{K_2}\theta_{H^*}^2$
3	$CAL^* + H^* \rightleftharpoons MS1^* + *$	$r_3 = k_3\theta_{cal^*}\theta_{H^*} - \frac{k_3}{K_3}\theta_1\theta_*$
4	$MS1^* + H^* \rightleftharpoons COL^* + *$	$r_4 = k_4\theta_1\theta_{H^*} - \frac{k_4}{K_4}\theta_{col^*}\theta_*$
5	$CAL^* + H^* \rightleftharpoons MS2^* + *$	$r_5 = k_5\theta_{cal^*}\theta_{H^*} - \frac{k_5}{K_5}\theta_2\theta_*$
6	$MS2^* + H^* \rightleftharpoons COL^* + *$	$r_6 = k_6\theta_2\theta_{H^*} - \frac{k_6}{K_6}\theta_{col^*}\theta_*$
7	$CAL^* \rightleftharpoons COL + *$	$r_7 = k_7\theta_{col^*} - \frac{k_7}{K_7}\frac{p_{col}}{p^\circ}\theta_*$

The standard molar translational entropy follows [65]:

$$S^\circ_{\text{trans-3D}} = R\left[\ln\left(\frac{(2\pi m k_B T)^{3/2}}{h^3}\right) + \ln\left(\frac{V}{N_g}\right) + \frac{5}{2}\right] \quad (6)$$

where m is the mass of the molecule and V/N_g is the volume per molecule in the standard state. For a nonlinear molecule, the standard molar rotational internal energy contribution is

$$U^\circ_{\text{rot}} = \frac{3}{2}RT \quad (7)$$

The standard molar rotational entropy contribution is

$$S^\circ_{\text{rot}} = R\left[\ln\left(\frac{8\pi^2\sqrt{8\pi^3 I_x I_y I_z}(k_B T)^{3/2}}{\sigma h^3}\right) + \frac{3}{2}\right] \quad (8)$$

where I_x, I_y, and I_z are the three moments of inertia about the principal axes and σ is the rotational symmetry number.

If it is a linear gaseous molecule, the corresponding standard molar internal energy and entropy contribution are

$$U^\circ_{\text{rot}}(\text{linear}) = RT \quad (9)$$

$$S^\circ_{\text{rot}}(\text{linear}) = R\left[\ln\left(\frac{8\pi^2 I(k_B T)}{\sigma h^2}\right) + 1\right] \quad (10)$$

respectively, where I is the moment of inertia of the linear molecule.

The molar enthalpy correction with respect to the internal energy is in the following expression:

$$H^\circ = U^\circ + \gamma RT \quad (11)$$

γ equals 1 for the gaseous molecule, and 0 for surface adsorbates. Thus, the standard molar Gibbs free energy change for each surface elementary reaction is calculated as

$$\Delta G^\circ = \Delta E + \Delta\text{ZPE} + \gamma RT + \Delta U^\circ - T\Delta S^\circ \quad (12)$$

where ΔE denotes as the total energy change from DFT calculation. The detailed treatments of adsorption and desorption rates are discussed in Section 3.

2.3. Microkinetic model

The microkinetic model based on a mean-field treatment is developed in terms of free energies for each elementary reaction (Table 1). In our microkinetic model, the reactor was simulated using the ideal continuous-stirred tank reactor (CSTR). The model parameters were set to follow the catalytic experiment work of Marinelli et al. [66], including the reactant flow rate of 2.09×10^{17} molecules/s, a catalyst area of 1 m^2 with a site concentration of 2.72×10^{-9} mol/m^2 and a reactor volume of 1×10^{-6} m^3. The model was implemented at 353 K with the mixture of crotonaldehyde (33 mbar) and hydrogen (978 mbar) pressure under the total pressure of 20 bar. The complete set of time-dependent CSTR differential algebraic equations listed in Tables 2 and 3 is solved using Mathematica.

Table 2
Steady-state site balances of adsorbates and free sites for the microkinetic model.

$$\frac{d\theta_{cal^*}}{dt} = r_1 - r_3 - r_5 = 0$$
$$\frac{d\theta_H}{dt} = 2r_2 - r_3 - r_4 - r_5 - r_6 = 0$$
$$\frac{d\theta_1}{dt} = r_3 - r_4 = 0$$
$$\frac{d\theta_2}{dt} = r_5 - r_6 = 0$$
$$\frac{d\theta_{col^*}}{dt} = r_4 + r_6 - r_7 = 0$$

3. Results and discussions

3.1. Reaction pathways in the free energy landscape

3.1.1. Chemisorption energy

In this study, we define the adsorption energies from DFT calculations in the following equation:

$$E_{\text{ad}} = E\left(\frac{\text{adsorbates}}{\text{metal}}\right) - E(\text{adsorbates}) - E(\text{metal}) \quad (13)$$

where each energy term on the right-hand side of equation comes from periodic DFT calculations. The desorption energies equal to the negative values of the corresponding adsorption energies. For the adsorbates, the molar Gibbs free adsorption energies at reaction temperature 353 K and under the standard pressure are as follows:

$$G_{\text{ad}}(T) = E_{\text{ad}} + \Delta\text{ZPE} + \Delta U + RT - T\Delta S(T) \quad (14)$$

where ΔZPE, ΔU and $\Delta S(T)$ denote the changes of zero-point-energy, internal energy and entropy during the adsorption process, respectively.

In the free energy landscape, *E*-(s)-trans-crotonaldehyde is favored in the gas phase with 0.09 eV more stable than *E*-(s)-cis, the second most stable one. On Pt(1 1 1) the adsorption structure of crotonaldehyde, trans-tetra-σ (the molecule adsorbs on Pt surface with trans geometry via C,C,C,O numbered in Scheme 1), is identified with the most stable configuration. Despite a large adsorption energy (−0.79 eV), trans-tetra-σ crotonaldehyde does not easily adsorb on Pt(1 1 1) in terms of the Gibbs free adsorption energy. In fact, the adsorbate is slightly less stable (0.04 eV) than the gas-phase molecule in the free energy landscape. This mainly arises from a large entropy loss of the adsorbate with respect to gaseous crotonaldehyde, in which the decrease of the translational and rotational contribution from the gas phase to the adsorbed state plays a major role. Conversely, as shown in Table 4, the free adsorption energy difference (0.31 eV) between hydrogen and crotonaldehyde due to the small rotational modes contribution of H_2 indicates that crotonaldehyde would occupy the surface sites

Table 3
Material balances for the gas-phase species within the microkinetic model applied to a steady state CSTR. N_x and F_x, in are the molar number and inlet flow rates of species x. A_s, ρ_s and t_{res} denote the catalysis area, the site concentration of catalysis and residence time, respectively.

$$\frac{dN_{cal}}{dt} = A_s\rho_s(-r_1) + \left(F_{cal,in} - \frac{N_{cal}}{t_{res}}\right)$$
$$\frac{dN_{H_2}}{dt} = A_s\rho_s(-r_2) + \left(F_{H_2,in} - \frac{N_{H_2}}{t_{res}}\right)$$
$$\frac{dN_{col}}{dt} = A_s\rho_s r_7 - \frac{N_{col}}{t_{res}}$$

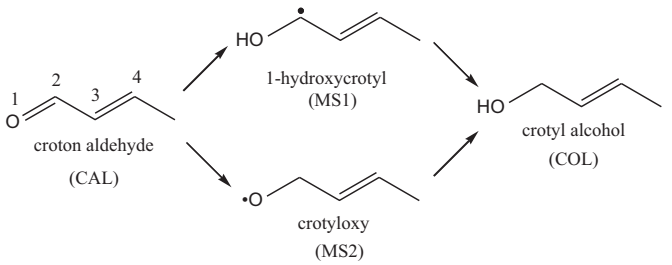

Scheme 1. Chemoselective hydrogenation pathways of trans-crotonaldehyde (CAL) to crotyl alcohol (COL) on Pt(1 1 1). The four possible hydrogen attacking sites are numbered from 1 to 4, corresponding O1, C2, C3, C4, respectively. Two possible first hydrogenation intermediates to yield COL, 1-hydroxycrotyl (MS1) and crotyloxy (MS2), are shown.

with a low coverage under the reaction condition. Accordingly, it is likely that the coverage of subsequent hydrogenation intermediates from crotonaldehyde is low. The intermediates MS1 and MS2 were found to adsorb on the surface with trans-tri-σ configuration via C2–C3–C4 and O1–C3–C4, respectively. The adsorption energy of MS2 is higher mainly because of its instability in the gas phase (radical). For the product COL, its adsorption energy is close to CAL, but 0.17 eV greater in the free energy landscape, implying that COL* (the species name followed by * denotes the species adsorbed on the surface) is slightly harder to desorb from the surface relative to the adsorbed reactant CAL*.

3.1.2. Surface hydrogenation pathways

Crotyl alcohol can be accessible via 1,2 addition, the hydrogenation of carbonyl bond, from two symmetric pathways: +12 or +21 hydrogenation on the surface. The reaction pathway beginning with the trans-tetra-σ configuration is presented hereinafter [47].

In the +12 hydrogenation pathway, the direct hydrogenation of crotonaldehyde on O1 yields MS1* via TS1* with a 0.52 eV free energy barrier. At TS1*, the hydrogen diffuses from the most stable 3-fold fcc site to the top site. The C=O fragment of CAL loses the bonding of the surface and di-σ-CC configuration is formed. The O–H distance is 1.368 Å and it corresponds to a stronger imaginary vibrational frequency, 808.0 cm^{-1}. The free energy barrier is almost identical with the energy barrier (0.50 eV), which means that the components of ZPE, internal energy and entropy mutually cancel out. The barrier is slightly higher than the corresponding hydrogenation result (0.41 eV) on acrolein with PW91 functional [46–48]. Because of the C=C–C• conjugate configuration of MS1*, the first hydrogenation step is exothermic, which assists the decrease of the barrier. MS1* is subsequently hydrogenated on C2 to form COL* via TS12*, corresponding to a 0.77 eV free energy barrier. At TS12*, the tri-σ configuration transforms to the di-σ-CC configuration with H on the top site originally occupied by C2. The C–H bond distance is 1.771 Å and the imaginary vibrational frequency is 531.3 cm^{-1}. The free energy barrier is higher than that of the first step hydrogenation. On the one hand, the hydrogenation of MS1* to COL* is an endothermic step resulting from the break of the conjugate structure. On the other hand, the higher electronegativity of O than that of C might intensify the interaction between O and H, which stabilizes the TS1. This is supported by the vibrational frequency result: a higher imaginary vibrational frequency of TS1* than TS12* was observed.

In the +21 hydrogenation pathway, firstly H attacks the C2 via TS2* to yield MS2*. Similarly, at TS2* H occupies the on-top site and forces C2 away from the surface. Without the stable conjugate configuration, MS2* is far less stable than MS1*. Naturally, the corresponding TS2* is 0.17 eV higher than TS1*. In the free energy profile, the free energy of TS2* is close to MS2* and the free energy barrier for TS21* is not high (0.37 eV). It indicates that MS2* is a transient intermediate, with a very low coverage on the surface. Since TS21* is 0.39 eV higher than TS12*, it implies that the +21 addition is a less favorable pathway to yield COL.

Table 4
Adsorption energies (E_{ad}) and free adsorption energies (G_{ad}) at 353 K under the standard pressure for intermediates on Pt(1 1 1). Adsorption energies with and without the zero-point-energy (ZPE) correction are given. The adsorption energy of H is with respect to gaseous $1/2H_2$. The unit is eV.

Species	E_{ad}		G_{ad}
	Without ZPE	With ZPE	
H	−0.47	−0.46	−0.27
CAL	−0.79	−0.77	0.04
MS1	−1.84	−1.81	−0.98
MS2	−2.14	−2.12	−1.28
COL	−0.84	−0.84	−0.13

3.1.3. The TSs of adsorption/desorption in the free energy landscape

Since adsorption and the corresponding desorption are the mutually time-reversed processes, they have to follow the principle of detailed balance or microscopic reversibility. This principle assures that the same TS exists for the forward and reverse processes between the gas phase and adsorbed state along minimum energy path in the free energy landscape, and the rate constants of adsorption k_{ad} and desorption k_{des} are related as follows:

$$\frac{k_{ad}}{k_{des}} = e^{-\Delta G^\circ/RT} = K_{eq} \tag{15}$$

where ΔG° denotes as the standard molar Gibbs free energy change between the molecule in the gas phase and the adsorbate, and K_{eq} is the corresponding reaction equilibrium constant.

In the total energy landscape (0 K), adsorption is a barrierless process for most of the systems, whereas in the free energy one, an apparent free energy barrier exists because of the evidently different translational or rotational modes between the gas phase and TS. Accurate calculations of free energy barriers are difficult, which have to turn to highly time-consuming ab initio dynamical simulations with statistically meaningful number of trajectories. This is beyond the scope of the present paper. Two alternative models with the same total energy of TS as the gas-phase molecule are commonly used [67] to obtain it: mobile and immobile models (or termed as indirect and direct [67], precursor and non-precursor [68]), in which different degrees of freedom are assumed.

In the mobile model, the molecule does not directly fix at the adsorption site. It first forms the TS with a weakly bound precursor state, in which it diffuses freely over the 2D surface, until it bonds with an adsorption site. The standard molar translational internal energy and entropy contribution of TS are

$$U^\circ_{trans\text{-}2D} = RT \tag{16}$$

$$S^\circ_{trans\text{-}2D} = R\left[\ln\left(\frac{2\pi m k_B T}{h^2}\right) + \ln C_{sites} + 2\right] \tag{17}$$

respectively, where C_{sites} is the surface concentration of sites. The standard molar rotational internal energy and entropy contribution are calculated in the same as those in 3D space. The vibrational contributions of adsorption/desorption TSs are calculated in the same way as those of the adsorbates except that three modes are removed: two frustrated translational modes reduced from the translational modes of gas-phase molecule along the surface and one from the reaction coordinate. In addition, there is no molar enthalpy correction with respect to the internal energy like the adsorbates.

The immobile model is one in which the gas-phase molecule collides with the surface and directly forms a TS sticking to the

adsorption site, and therefore only vibrational contribution including two frustrated translational and three rotational modes reduced from translational and rotational modes of gas-phase molecule is involved in the free energy calculation of TS. The vibrational contributions of adsorption/desorption TSs follow the same approach as those of the adsorbates except that the vibrational mode of the reaction coordinate is excluded. Due to more degrees of freedom, the free energy barrier of TS in the mobile model is usually lower than that in the immobile model. Real adsorption TSs generally locate between these two ideal limits [67].

In addition to the mobile and immobile models, the collision theory is another conventional approach to describe the adsorption processes, in which the molecules are assumed to randomly impinge the surfaces with the Maxwell–Boltzmann distributed velocities. The adsorption rate constant under the standard pressure p° is determined by

$$k_{ad} = S_0(T)\frac{p^\circ}{N_0\sqrt{2\pi m k_B T}} \quad (18)$$

where $S_0(T)$ is the initial sticking coefficient on a clean surface from experiment study, and N_0 is Avogadro constant. The equation of collision theory is able to be converted in the form of TST [67]. Therefore, the apparent free energy barrier for TST can be derived from the known initial sticking coefficients. Following detailed balance and Eq. (18), the adsorption and the corresponding desorption free energy barrier are

$$\Delta G_{ad}^{\neq,\circ} = -RT\ \ln\ \frac{h}{k_B T}\frac{S_0(T)p^\circ}{N_0\sqrt{2\pi m k_B T}} \quad (19)$$

$$\Delta G_{des}^{\neq,\circ} = -\Delta G^\circ - RT\ \ln\ \frac{h}{k_B T}\frac{S_0(T)p^\circ}{N_0\sqrt{2\pi m k_B T}} \quad (20)$$

As mentioned above, we investigated the adsorption/desorption free energy barriers of reactants and products based on the mobile model, immobile model and the value derived from collision theory, respectively. The detailed adsorption/desorption free energy barriers with different treatments are listed in Table 5. For the values derived from collision theory, the initial sticking coefficients for H_2 were selected according to the experiment data 0.046 [69]. There is no published experiment data of CAL and COL initial sticking coefficients on Pt(1 1 1). However, it is reasonable to assume that their values are close to those of similar molecules, 3-methylcrotonaldehyde and 3-methyl-crotyl alcohol [70], which possess the initial sticking coefficients of 0.6 and 0.5, respectively. Their corresponding adsorption free energy barriers are similar, both 0.36 eV.

Table 5
Adsorption free energy barrier $\Delta G_{ad}^{\neq,\circ}$ and desorption free energy barrier $\Delta G_{des}^{\neq,\circ}$ at 353 K under the standard pressure for intermediates on Pt(1 1 1) with different model calculations. The unit is eV.

	$\Delta G_{ad}^{\neq,\circ}$			$\Delta G_{des}^{\neq,\circ}$		
	CAL	H_2	COL	CAL	H_2	COL
Mobile	0.34	0.29	0.34	0.30	0.73	0.47
Immobile	0.82	0.40	0.71	0.78	0.94	0.84
CT	0.36	0.38	0.36	0.32	0.92	0.49

Table 5 shows that, irrespective of the model, non-zero adsorption free energy barriers for all molecules do exist. This is in contrast to the barrierless adsorption in the total energy landscape (0 K) and shows that the entropic effect is actually important to the adsorption process. Similar differences are found for the reverse desorption process. In addition, the adsorption free energy barriers from the collision theory model are actually located between the mobile and immobile model. The adsorption free energy barriers of CAL and COL from collision theory model are fairly close to the mobile model (Table 5). Although the adsorption free energy barrier of H_2 from experiment is closer to that of immobile model, the difference between the free energy barriers from mobile and immobile models is marginal. It implies that the mobile model is likely to be close to the experimental work. Moreover, it is interesting that the desorption barriers for COL in the free energy profile are only 0.47 and 0.49 eV from the mobile model and collision theory model, respectively, which are close to half of that in the total energy profile (0.90 eV), indicating that the entropy change greatly reduces the difficulty in COL desorption. Thus, the desorption step of COL may not be as critical as expected in the total energy landscape (0 K). As Fig. 1 shows, the stability of TS12* is quite close to that of the TS of COL* desorption rather than the TS of COL* desorption which is far less stable in the total energy profile [48]. This

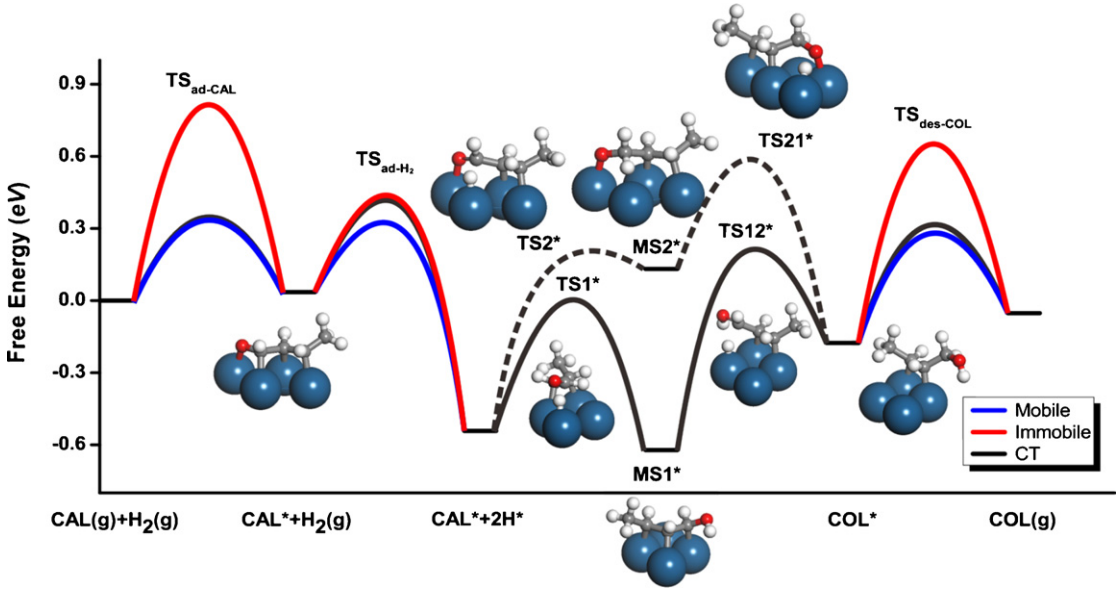

Fig. 1. Free energy profile of chemoselective hydrogenation on trans-crotonaldehyde (CAL) to crotyl alcohol (COL) over Pt(1 1 1) with respect to gas-phase trans-crotonaldehyde and hydrogen. The adsorption/desorption free energy barriers calculated in three different methods: mobile, immobile model and collision theory (CT) model are shown. Two alternative pathways, +12 and +21 hydrogenation, are displayed.

Table 6
Comparisons of the free energy changes (ΔG°), total energy changes (ΔE), ZPE changes (ΔZPE), internal energy changes (ΔU°) and entropy change ($-T\Delta S^\circ$) for the each elementary step in the surface hydrogenation process at 353 K. The unit is eV.

Step i	ΔG°	ΔE	ΔZPE	ΔU°	$-T\Delta S^\circ$	$\Delta U^\circ - T\Delta S^\circ$
3	−0.104	−0.313	0.162	−0.018	0.066	0.048
4	0.681	0.500	0.115	−0.031	0.098	0.066
5	0.327	0.243	0.171	0.014	−0.101	−0.087
6	−0.457	−0.570	0.218	0.027	−0.133	−0.105

indicates that it is the balance between the second hydrogenation and the COL* that determines the yield of COL(g) and then the selectivity. In the immobile model, due to the similar entropies between the IS and the TS in which only vibrational modes remain, the free energy barrier of COL desorption (0.84 eV) is similar to that in the total energy landscape. As displayed in Fig. 1, the trivial entropic effect leads to the result that this desorption free energy barrier from the immobile model is much larger than those from the mobile and collision theory models. This indicates that the significance of the adsorption/desorption process for the entire reaction system is likely to be overestimated if the immobile model is used. We also found that regardless of the calculated methods, the adsorption free energy barriers of CAL and COL are similar, suggesting that the role of adsorption/desorption step of CAL played in the reaction system is no less than the adsorption/desorption step of COL. Furthermore, as Fig. 1 depicted, the TS of CAL adsorption, especially in the immobile model, is not only the highest point in the entire free energy profile but also far more higher than the TS of the surface hydrogenation process. This implies that the adsorption of CAL may be the crucial step to determine the entire reaction rate for the immobile model. The adsorption/desorption process will be further discussed using microkinetic analysis in Section 3.3.

3.2. ZPE corrections, thermal energies correction and entropies effect

In addition to the investigation of the difference between the total energy and the free energy landscape for the adsorption/desorption processes, we also probed the difference between the total energy and the free energy landscape as well as the effect of each energy component constituting the free energy for the surface hydrogenation processes. During the surface hydrogenation procedure, although the vibrational contribution for each species on the surface is not small (0.23 eV of average internal energy and 0.43 eV of entropy for each intermediate and TS except H*, Table S2), it is clear that the internal energy intrinsically wipes out a part of the entropy effect derived from Eqs. (3) and (4):

$$\begin{aligned} U^\circ_{\mathrm{vib}} - \mathrm{TS}^\circ_{\mathrm{vib}} &= RT\sum_i \frac{h\nu_i/k_{\mathrm{B}}}{e^{h\nu_i/k_{\mathrm{B}}T}-1} \\ &\quad -RT\sum_i \left[\frac{h\nu_i/k_{\mathrm{B}}T}{e^{h\nu_i/k_{\mathrm{B}}T}-1} - \ln(1-e^{-h\nu_i/k_{\mathrm{B}}T})\right] \\ &= RT\sum_i \ln(1-e^{-h\nu_i/k_{\mathrm{B}}T}) \end{aligned} \quad (21)$$

The mutual cancellation makes them only about 0.20 eV overall contribution to each species.

Furthermore, from Tables 6 and 7, $\Delta U^\circ - T\Delta S^\circ$ terms are around 0.06 eV (the maximum is 0.105 eV) under the reaction condition. Both the internal energies and entropies of different intermediates and TSs are so similar that the total contributions from the internal energy and entropy changes for the reaction energy and barrier almost vanish. Moreover, the $\Delta U^\circ - T\Delta S^\circ$ terms cancel to a large extent each other due to the fact that their values alternate between positive and negative. This indicates the error without this term will not considerably enlarge with the increasing reaction step. The internal energy and entropy contributions are trivial for the surface process at current temperature. Nevertheless, since $\Delta U^\circ - T\Delta S^\circ$ term is proportional to the temperature as Eq. (21) displayed, this contribution is likely not to be negligible at high temperatures.

Different from the internal energy and entropy components, as listed in Tables 6 and 7, it is likely that the ZPE correction should be important for the surface hydrogenation process. In each hydrogenation elementary step, the reaction energy increases by 0.1–0.2 eV with the ZPE correction. The energy barrier has a trivial change (average 0.015 eV). This smaller value mainly results from the fact that the structure of TS is close to that of IS during the hydrogenation process. The error of 0.1–0.2 eV may not be so significant to influence the reaction result (close to the intrinsic error of DFT). However, since the values are all positive, the error could continuously accumulate with the increment of the hydrogenation steps, leading to a greater error between the initial adsorbates and final hydrogenation products. As a result, for a multiple-step hydrogenation system, the calculation results such as the coverage of hydrogenation intermediates and the overall hydrogenation barrier with the ZPE correction will be apparently different from those without the ZPE correction. With the ZPE correction, the hydrogenation intermediates will be less stable with respect to calculations without the ZPE correction in the energy profile, giving rise to the increase of overall barrier and low coverage of subsequent hydrogenation product. In the reaction system addressed in the current work, it means that the full hydrogenation product will be fewer with the ZPE correction.

In order to manifest the effects discussed above, one of the full hydrogenation pathway from crotonaldehyde to 1-butanol (BOL) in the order of hydrogenation: O1, C2, C3 and C4 (+1234 hydrogenation) is shown in Fig. 2. It is clear from Fig. 2 that the final hydrogenation product BOL* with the correction of ZPE is 0.45 eV less stable than that without the ZPE correction. The overall barrier of four-step hydrogenation reactions with the ZPE correction is 0.48 eV higher than that without the ZPE correction. It can be

Table 7
Comparisons of the forward free energy barrier ($\Delta G^{\neq,\circ}$), forward activation energy barriers (E_a), ZPE changes (ΔZPE$^\neq$), internal energy changes ($\Delta U^{\neq,\circ}$) and entropy change ($-T\Delta S^{\neq,\circ}$) between TS and IS for the each elementary step in the surface hydrogenation process at 353 K under the standard pressure. The unit is eV.

Step i	$\Delta G^{\neq,\circ}$	E_a	ΔZPE$^\neq$	$\Delta U^{\neq,\circ}$	$-T\Delta S^{\neq,\circ}$	$\Delta U^{\neq,\circ} - T\Delta S^{\neq,\circ}$
3	0.517	0.503	−0.015	−0.017	0.046	0.029
4	0.693	0.606	0.013	−0.034	0.109	0.074
5	0.767	0.773	0.004	−0.002	−0.009	−0.011
6	0.373	0.305	0.057	−0.010	0.022	0.011

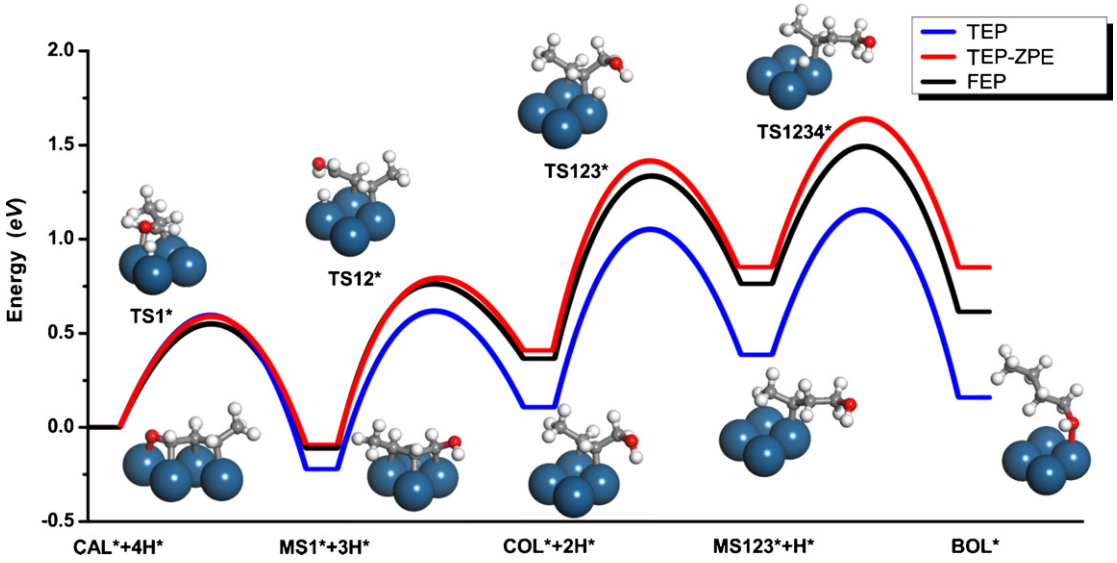

Fig. 2. Free energy profile (FEP), total energy profile with the zero-point-energy correction (TEP-ZPE) and without the zero-point energy correction (TEP) of chemoselective hydrogenation from adsorbed trans-crotonaldehyde (CAL) to 1-butanol (BOL) over Pt(1 1 1) via +1234 pathway with respect to the corresponding CAL energy.

inferred that the yield of BOL using the DFT data with the ZPE will be far lower than that without the ZPE. In the meantime, compared to the values in the free energy profile, the error of overall barrier from total energy with the ZPE correction is reduced to 0.15 eV, much less than that without the ZPE correction (0.33 eV). Hence, according to the quantitative analysis above, the energy calculation from DFT with the ZPE correction is close to the full free energy calculation for the surface reaction except at high temperatures.

This should be true for the other reaction systems with multiple-step hydrogenation reaction. For instance, for the FT reaction, firstly the overall hydrogenation barrier from C* to CH_4 obtained from calculations with the ZPE correction will be 0.3–0.5 eV higher than those without the ZPE correction. Secondly, greater coverage of C* will be obtained, implying a higher possibility of C–C coupling reaction with respect to the results from the profile without ZPE correction. This may lead to a modification of the understanding of the reaction mechanism of FT.

3.3. Microkinetic simulations and analysis

In order to identify the dominate pathway and to evaluate the turnover frequency (TOF) of the reaction network to yield COL, the microkinetic model was built on the data obtained from DFT and statistical treatment in the previous sections. The reaction rate constants derived from TST in terms of free energies are imported into the model. No assumption as to the rate-determining step was made. The simulated surface coverages and turnover frequency (TOF) of COL were achieved at steady state from our model.

The TOF calculations and kinetic analyses corresponding to the three different methods of adsorption/desorption free energy barriers (mobile, immobile and collision theory) were carried out. The results are summarised in Tables 8 and 9. It is clear from Tables 8 and 9 that the results from the mobile and collision theory models are very close to each other, owing to the similar adsorption/desorption free energy barriers. Their TOFs are 6.81×10^{-3} and 6.78×10^{-3} s^{-1}, respectively, 2 orders of magnitude larger than the immobile model. The TOF from experiment is about 0.01–0.1 s^{-1} [40,71]. It indicates that the results from the mobile and collision theory models fit the experiment result better.

In addition, as shown in Tables 8 and 9, the results of the dominant reaction pathway and the surface species coverage are in good agreement in all the three methods. The COL is almost solely produced via the +12 hydrogenation pathway with a TOF which is 4 orders of magnitude larger compared with the contribution from the +21 hydrogenation pathway. Obviously, the +12 hydrogenation pathway is the dominant pathway to generate COL(g). As shown in Table 8 from the microkinetic simulation, H* is the dominant species on Pt(1 1 1). Second to H*, MS1* makes up a certain proportion of the surface species by virtue of its advantage of both kinetics (the lower free energy barrier of its generation, 0.55 eV) and thermodynamics (its location on the bottom of the whole free energy profiles, Fig. 1). The coverage of CAL* is low, mainly due to the swift conversion of adsorbed CAL* to MS1* on the surface apart from the competitive adsorption with H_2. The coverage of MS2* is very low, which is consistent with its characteristic of transient intermediate as shown in Fig. 1.

Finally, the calculated surface coverages of all the intermediates except H* from the immobile model are clearly lower than those from the mobile and collision theory models, ultimately leading to the low TOF from this model. The higher adsorption free energy barrier of CAL (0.82 eV, Table 5) instead of the higher desorption free energy barrier of COL could account for this result. When the adsorption of CAL is rate-determining step in the reaction system, the higher free energy barrier of its adsorption will

Table 8
Surface coverage of intermediates at steady state under the reaction conditions using three different treatments of adsorption/desorption free energy barrier.

Species	θ_n (ML^{-1})		
	Mobile	Immobile	CT
CAL*	5.61×10^{-7}	2.94×10^{-8}	5.67×10^{-7}
H*	9.52×10^{-1}	9.97×10^{-1}	9.51×10^{-1}
MS1*	4.78×10^{-2}	2.82×10^{-3}	4.82×10^{-2}
MS2*	1.07×10^{-12}	5.65×10^{-14}	1.07×10^{-12}
COL*	1.72×10^{-4}	1.04×10^{-5}	1.71×10^{-4}

Table 9
Calculated TOF of the product COL from two different hydrogenation pathways.

	TOF (s^{-1})	
	+12	+21
Mobile	6.81×10^{-3}	2.84×10^{-7}
Immobile	6.50×10^{-5}	2.78×10^{-9}
CT	6.78×10^{-3}	2.81×10^{-7}

lead to the low coverage of CAL* and the further low coverage of intermediates initiating from CAL*. Conversely, the higher desorption free energy barrier of COL would increase the difficulty of the product desorption, only resulting in the increase of the surface coverage of product in the case that the desorption step of the product is the key step of the reaction. It is intriguing that our results show the reactant adsorption instead of the product desorption being crucial to the reaction from the immobile model in which the desorption free energy barrier is close to the energy barrier. As the TOF from immobile model is 3 or 4 orders of magnitude smaller than the experimental results, the immobile model may overestimate the free energy barriers of adsorption/desorption processes.

4. Conclusions

In the present work, microkinetic model was developed based on free energy to investigate the reaction mechanism of crotonaldehyde partial hydrogenation to crotyl alcohol over Pt(1 1 1). The statistical thermodynamic treatment involving ZPE correction, internal energy and entropy effect based on DFT-derived energy was applied to obtain the Gibbs free energy throughout all the elementary steps under the reaction condition.

Three different methods (mobile, immobile and collision theory models) were used to obtain free energy barrier of adsorption/desorption process and the corresponding kinetic results were analyzed, respectively. The results from the mobile and collision theory models are similar, from which TOFs are close to the experiment value. However, for the immobile model, in which the desorption free energy barrier with little entropic effect approaches the energy barrier, the calculated TOF is 2 orders of magnitude lower than the other models. The difficulty of adsorption/desorption may be overestimated in immobile model.

Based on the analysis, it supports the idea that the total energy with the ZPE correction approaches the full free energy calculation for the surface reaction in the low or mild temperature. During the surface hydrogenation elementary steps, under the investigated conditions, the entropy and internal energy effects are of little importance since the changes of them almost cancelled each other. The ZPE correction is small for the free energy barrier calculation, but it is 0.1–0.2 eV for the reaction energy in each elementary step. Because of the accumulation effect, the ZPE correction will be an important component of overall barrier and reaction energy between initial reactant and final multi-step hydrogenation product in multi-step hydrogenation reaction.

Acknowledgment

We gratefully acknowledge The Queen's University of Belfast for computing time. X.-M. C. thanks The Queen's University of Belfast for a Ph.D. studentship.

Appendix A. Supplementary data

Supplementary data associated with this article can be found, in the online version, at doi:10.1016/j.cattod.2010.12.056.

References

[1] M.A. Vannice, Catal. Rev. – Sci. Eng. 14 (1976) 153–191.
[2] P. Biloen, W.M.H. Sachtler, Adv. Catal. 30 (1981) 165–216.
[3] E. Iglesia, Appl. Catal. A 161 (1997) 59–78.
[4] H. Schulz, Appl. Catal. A 186 (1999) 3–12.
[5] H. Schulz, M. Claeys, Appl. Catal. A 186 (1999) 91–107.
[6] M.E. Dry, Catal. Today 71 (2002) 227–241.
[7] J. Cheng, P. Hu, P. Ellis, S. French, G. Kelly, C.M. Lok, J. Phys. Chem. C 112 (2008) 6082–6086.
[8] J. Cheng, X.-Q. Gong, P. Hu, C.M. Lok, P. Ellis, S. French, J. Catal. 254 (2008) 285–295.
[9] J. Cheng, P. Hu, P. Ellis, S. French, G. Kelly, C.M. Lok, J. Catal. 257 (2008) 221–228.
[10] J. Cheng, P. Hu, P. Ellis, S. French, G. Kelly, C.M. Lok, J. Phys. Chem. C 254 (2009) 8858–8863.
[11] O. Hinrichsen, F. Rosowski, A. Hornung, M. Muhler, G. Ertle, J. Catal. 165 (1997) 33–44.
[12] H. Dietrich, K. Jacobi, G. Ertle, J. Chem. Phys. 106 (1997) 9313–9319.
[13] S. Dahl, P.A. Taylor, E. Törnqvist, I. Chorkendorff, J. Catal. 178 (1998) 679–686.
[14] S. Hagen, R. Barfod, R. Fehrmann, C.J.H. Jacobsen, H.T. Teunissen, I. Chorkendoff, J. Catal. 214 (2003) 327–335.
[15] A. Logadóttir, J.K. Nørskov, J. Catal. 220 (2003) 273–279.
[16] S.E. Siporin, R.J. Davis, W. Raróg-Pilecka, D. Szmigiel, Z. Kowalczyk, Catal. Lett. 93 (2004) 61–65.
[17] K. Bauer, D. Garbe, Common Fragrance and Flavor Materials, Wiley-VCH, Weinheim, 1985.
[18] K. Bauer, D. Garbe, Ullman Encyclopedia, Wiely-VCH, New York, 1988.
[19] K. Weissermel, H.J. Arpe, Industrial Organic Chemistry, Verlag Chemie, Weinheim, 1978.
[20] P. Gallezot, D. Richard, Catal. Rev. – Sci. Eng. 40 (1998) 81–126.
[21] V. Ponec, Appl. Catal. A 149 (1997) 27–48.
[22] P. Mäki-Arvela, J. Hájek, T. Salmi, D.Yu. Murzin, Appl. Catal. A 292 (2005) 1–49.
[23] M.L. Toebes, F.F. Prinsloo, J.H. Bitter, A.J. van Dillen, K.P. deJong, J. Catal. 214 (2003) 78–87.
[24] A.M. Silva, O.A.A. Santos, M.J. Mendes, E. Jordaõ, M.A. Fraga, Appl. Catal. A 241 (2003) 155–165.
[25] M. Lashdaf, M. Tiitta, T. Venäläinen, H. Österholm, A.O.I. Krause, Catal. Lett. 94 (2004) 7–14.
[26] J. Hájek, N. Kumar, T. Salmi, D.Yu. Murzin, Ind. Eng. Chem. Res. 42 (2003) 295–305.
[27] B. Bachiller-Baeza, I. Rodríguez, A. Guerrero-Ruiz, Appl. Catal. A 205 (2001) 227–237.
[28] L. Sordelli, R. Psaro, G. Vlaic, A. Cepparo, S. Recchia, C. Dossi, A. Fusi, R. Zanoni, J. Catal. 182 (1999) 186–198.
[29] P. Mastrorilli, A. Rizzuti, G.P. Suranna, C.F. Nobile, Inorg. Chim. Acta 304 (2000) 17–20.
[30] I. Bergault, P. Fouilloux, C. Joly-Vuillemin, H. Delmas, J. Catal. 175 (1998) 328–337.
[31] P. Reyes, G. Pecchi, J.L.G. Fierro, Langmuir 17 (2000) 522–527.
[32] P. Reyes, M.C. Aguirre, J.L.G. Fierro, G. Santori, O. Ferretti, J. Mol. Catal. A: Chem. 184 (2002) 431–441.
[33] A. Dandekar, M.A. Vannice, J. Catal. 183 (1999) 344–354.
[34] J. Aumo, J. Lilja, P. Mäki-Arvela, T. Salmi, M. Sundell, H. Vainio, D.Yu. Murzin, Catal. Lett. 84 (2002) 219–224.
[35] P. Claus, A. Brückner, C. Morh, H. Hofmeister, J. Am. Chem. Soc. 122 (2000) 11430–11439.
[36] C. Mohr, H. Hofmeister, J. Radnik, P. Claus, J. Am. Chem. Soc. 125 (2003) 1905–1911.
[37] U.K. Singh, M.A. Vannice, Appl. Catal. A 213 (2001) 1–24.
[38] U.K. Singh, M.A. Vannice, J. Catal. 191 (2000) 165–180.
[39] F. Ammari, J. Lamotte, R. Touroude, J. Catal. 221 (2004) 32–42.
[40] M. Englisch, A. Jentys, J.A. Lercher, J. Catal. 166 (1997) 25–35.
[41] M. Englisch, V.S. Ranabe, J.A. Lercher, Appl. Catal. A 163 (1997) 111–122.
[42] D.V. Sokolskii, N.V. Anisimova, A.K. Zharmagambetova, S.G. Mukhamedzhanova, L.N. Edygenova, React. Kinet. Catal. Lett. 33 (1987) 399–403.
[43] T.B.L.W. Marinelli, V. Ponec, J. Catal. 156 (1995) 51–59.
[44] F. Delbecq, P. Sautet, J. Catal. 152 (1995) 217–236.
[45] F. Delbecq, P. Sautet, J. Catal. 211 (2002) 398–406.
[46] D. Loffreda, F. Delbecq, F. Vigne, P. Sautet, J. Am. Chem. Soc. 128 (2006) 1316–1323.
[47] D. Loffreda, F. Delbecq, F. Vigne, P. Sautet, Angew. Chem. Int. Ed. 44 (2005) 5279–5282.
[48] S. Laref, F. Delbecq, D. Loffreda, J. Catal. 265 (2009) 35–42.
[49] I.G. Pitt, R.G. Gilbert, K.R. Ryan, J. Phys. Chem. 98 (1994) 13001–13010.
[50] I.G. Pitt, R.G. Gilbert, K.R. Ryan, Surf. Sci. 324 (1995) 69–89.
[51] L.C. Grabow, A.A. Gokhae, S.T. Evans, J.A. Dumesic, M. Mavrikakis, J. Phys. Chem. C 112 (2008) 4608–4617.
[52] O.R. Inderwildi, S.J. Jenkins, D.A. King, J. Am. Chem. Soc. 129 (2007) 1751–1759.
[53] D. Mei, Q. Ge, M. Neurock, L. Kieken, J. Erou, Mol. Phys. 102 (2004) 361–369.
[54] D.W. Blaylock, T. Ogura, W.H. Green, G.J.O. Beran, J. Phys. Chem. C 113 (2009) 4898–4908.
[55] J.P. Perdew, K. Burke, M. Ernzerhof, Phys. Rev. Lett. 77 (1996) 3865–3868.
[56] G. Kresse, J. Hafner, Phys. Rev. B 49 (1994) 14251–14269.
[57] G. Kresse, J. Furthmüller, Comput. Mater. Sci. 6 (1996) 15–50.
[58] G. Kresse, D. Joubert, Phys. Rev. B 59 (1999) 1758–1775.
[59] G. Henkelman, H. Jónsson, J. Chem. Phys. 111 (1999) 7010–7023.
[60] R.A. Olsen, G.J. Kroes, G. Henkelman, A. Arnaldsson, H. Jónsson, J. Chem. Phys. 121 (2004) 9776–9793.
[61] J. Kästner, P. Sherwood, J. Chem. Phys. 128 (2008) 14106–14112.
[62] E.K. Grimmelmann, J.C. Tully, E. Helfand, J. Chem. Phys. 74 (1981) 5300–5310.
[63] D.G. Truhlar, B.C. Garrett, S.J. Klippenstein, J. Phys. Chem. 100 (1996) 12771–12800.

[64] A.A. Gokhale, S. Kandoi, J.P. Greeley, M. Mavrikakis, J.A. Dumesic, Chem. Eng. Sci. 59 (2004) 4679–4691.
[65] R.D. Cortright, J.A. Dumesic, Adv. Catal. 46 (2001) 161–264.
[66] T. Marinelli, S. Nabuurs, V. Ponec, J. Catal. 151 (1995) 431–438.
[67] I. Chorkendorff, H. Niemantsverdriet, Concepts of Modern Catalysis and Kinetics, Wiley-VCH, Weinheim, 2003.
[68] D.J. Doren, J.C. Tully, Langmuir 4 (1988) 256–268.
[69] O. Deutschmann, R. Schmidt, F. Behrendt, J. Warnatz, Proc. Combust. Inst. 26 (1996) 1747–1754.
[70] T. Birchem, C.M. Pradier, Y. Berthier, G. Cordier, J. Catal. 146 (1994) 503–510.
[71] P. Claus, Top. Catal. 5 (1998) 51–62.